AGU PUBLICATIONS

JGR

Journal of Geophysical Research: Atmospheres

RESEARCH ARTICLE
10.1002/2015JD024126

Key Points:
- Rain rate variability increases as the length scale L increases
- For L (greater than) 1 km, this is due to the total number of drops, not the distribution of drop sizes
- For L (less than) 1 km, the distribution of drop sizes becomes increasingly important

Correspondence to:
A. R. Jameson,
arjatrjhsci@verizon.net

Citation:
Jameson, A. R., and M. L. Larsen (2016), The variability of the rainfall rate as a function of area, *J. Geophys. Res. Atmos.*, *121*, doi:10.1002/2015JD024126.

Received 23 AUG 2015
Accepted 21 DEC 2015
Accepted article online 29 DEC 2015

©2015. American Geophysical Union. All Rights Reserved.

The variability of the rainfall rate as a function of area

A. R. Jameson[1] and M. L. Larsen[2]

[1]RJH Scientific, Inc., El Cajon, California, USA, [2]Department of Physics and Astronomy, College of Charleston, Charleston, South Carolina, USA

Abstract Distributions of drop sizes can be expressed as DSD = $N_t \times$ PSD, where N_t is the total number of drops in a sample and PSD is the frequency distribution of drop diameters (D). Their discovery permitted remote sensing techniques for rainfall estimation using radars and satellites measuring over large domains of several kilometers. Because these techniques depend heavily on higher moments of the PSD, there has been a bias toward attributing the variability of the intrinsic rainfall rates R over areas (σ_R) to the variability of the PSDs. While this variability does increase up to a point with increasing domain dimension L, the variability of the rainfall rate R also depends upon the variability in the total number of drops N_t. We show that while the importance of PSDs looms large for small domains used in past studies, it is the variability of N_t that dominates the variability of R as L increases to 1 km and beyond. The PSDs contribute to the variability of R through the relative dispersion of $\chi = D^3 V_t$, where V_t is the terminal fall speed of drops of diameter D. However, the variability of χ is inherently limited because drop sizes and fall speeds are physically limited. In contrast, it is shown that the variance of N_t continuously increases as the domain expands for physical reasons explained below. Over domains larger than around 1 km, it is shown that N_t dominates the variance of the rainfall rate with increasing L regardless of the PSD.

1. Introduction

Anyone who has looked out a window as a storm passes knows how variable the rainfall rate can be on many different scales. Aside from intellectual curiosity, however, the variability of the rainfall rate is of practical concern for a better understanding of the worldwide multibillion dollar losses caused by soil erosion [*Uri and Lewis*, 1999], to mountain runoff planning [*Meusburger et al*., 2012], and to runoff and urban flood planning [*Smith et al*., 2004; *Sangati and Borga*, 2009]. These different concerns cover a wide range of scales from centimeters to several tens of kilometers. Some require small-scale detailed knowledge of the sizes of drops as for soil erosion physics [*Kinnell*, 2005; *Caracciolo et al*., 2012], while others such as planning for urban runoff are most interested in scales approaching several kilometers. For these latter concerns, it seems unlikely that details of drop sizes should matter, but can this be demonstrated?

Many mathematical-statistical approaches including fractals [*Lovejoy and Mandelbrot*, 1985] have been developed for modeling rainfall and its variability by treating the rain as a self-contained single variable such as the rainfall rate or total rainfall over some interval. To date, however, there are few approaches to modeling the variability of rain based upon the underlying microphysical variables of the rain itself, namely, drop sizes and drop numbers. As a step toward achieving this goal, *Kostinski and Jameson* [1999] showed that an obvious dichotomy of drop size distributions is the separation of the total number of drops from the probability distribution of drops of different sizes. That is, the drop size distribution, DSD = PSD $\times N_t$, where N_t it the total number of drops and the PSD is the probability or frequency distribution of the drop diameters. As a consequence of this separation, analyses by *Jameson and Kostinski* [2001, 2002] revealed the important role of N_t to the variability among integral parameters of the DSD. The purpose of this work, then, is to return to look at the fundamental physical properties of the DSD in order to develop a deeper, more physically based understanding of rainfall variability that could be potentially useful to the topics discussed above.

Ever since the first reports of DSD [*Laws and Parsons*, 1943; *Marshall and Palmer*, 1948; *Best*, 1950], the role they play with respect to the rainfall rate R has been a topic of intense research over the last several decades. Consequently, there was a growing appreciation of the variability of DSD particularly with regard to different meteorological conditions and for different R. It is not surprising, then, that the variability of R became inextricably linked to variations in the DSD. Furthermore, these associations were strengthened by numerical simulations of the microphysical processes which tended to focus on the intensive properties like changes to the drop sizes and the evolution of their distribution through the processes of diffusion, collision, coalescence,

and breakup rather than focusing on the extensive property of the number of drops which could be viewed as an extensive, somewhat adjustable parameter. It was natural, then, that the tendency has been to focus on the contribution of the PSD to the observed variability in R while tending to ignore the role of N_t. Certainly, the PSDs have been the primary concern in the development of rainfall retrievals using remote sensing algorithms.

Another contributing factor to this close attention to the PSD was that most if not all of these observations were made using single detectors having dimensions of less than a fraction of a meter. As we will show below, even having more than one detector in close proximity with another would likely have led to the same conclusion regarding the dominant role played by the PSD to a deeper understanding of the variability of R.

However, the rainfall rate is a function of two elements, the total number of drops, N_t, and the sizes of the drops, D_i. That is,

$$R = \sum_{i=1}^{N_t} \rho_w \frac{\pi D_i^3}{6} V_i(D_i) = \rho_w N_t \sum_{D_i} f(D_i, V_i) \frac{\pi D_i^3}{6} V(D_i) \tag{1}$$

where ρ_w is the density of water and $V_i(D)$ is the fall speed of the drops of diameter D; the summation is over all drops in a unit sample volume at some location and time, and $f(D_i,V_i)$ is the fraction of all the drops having diameter D_i and associated V_i.

To express this slightly differently, a drop size distribution can be described as the product of the total number of drops, N_t, times the probability distribution of drops with size, $P(D)\mathrm{d}D$, as argued in *Kostinski and Jameson* [1999], i.e., $N(D)\mathrm{d}D = N_t P(D)\mathrm{d}D$, where $P(D)\mathrm{d}D$ is the probability of finding a drop size between D and $D + \mathrm{d}D$. That is, $\mathrm{DSD} = N_t \times \mathrm{PSD}$, where $\mathrm{PSD} = P(D)\mathrm{d}D$. The variability in time and space of R, then, depends not just on the variability of, $\chi \equiv D^3 V_t$, but also upon the variability of N_t.

The importance of N_t has been recognized subsequently by *Uijlenhoet et al.* [2003] as well as by *Steiner et al.* [2004]. However, in both instances, the authors attempt to interpret their findings microphysically. We believe this may not be appropriate in part because of the limited number of drops sampled in each time interval and because of the limited size of the area of observations (usually just one instrument) which could mistakenly imply artificial correlations between the size distributions of diameters and N_t even though they are statistically independent [*Jameson and Kostinski*, 2002]. What this work shows is that while parameters such as the mean drop size are certainly influenced by microphysical processes, the number of drops is an independent variable which can overwhelm such microphysical influences when considering the rainfall rate variability over sufficiently large areas because of a smoothing over the drop size variability. That is, drop size variability is constrained over an area by the natural limits in the possible sizes of drops, whereas N_t has no such clear upper limit although eventually there must be. This will become clearer in a moment.

Developing a thorough knowledge of the variability of χ requires extensive research into the meteorological variability of drop size distributions, a topic well beyond the scope of this work. Here we have a much more limited objective, namely, that of relating the observed variability of R to the variability of χ and N_t and of exploring the relative importance of each as the size of the domain of observations increases. The relative dispersions are given by $\mathrm{RD}_{Nt} = \sigma_{Nt}/\langle N_t \rangle$ and $\mathrm{RD}_\chi = \sigma_\chi/\langle \chi \rangle$, where σ is the scale-dependent standard deviation of a variable and $\langle \cdot \rangle$ is its mean value. It is a natural quantity for measuring the variability of both χ and N_t.

Before proceeding, there are two noteworthy observations. First, χ is limited in the maximum values it can achieve so that its variability is also limited. That is, drop physics dictates that D can only be approximately 6–7 mm before instabilities lead to drop breakup. Likewise, V_t can only be about $10\,\mathrm{ms}^{-1}$ at most in still air. Consequently, their product must also be limited. On the other hand, there are no known equivalent limits for N_t dictated by physics alone although there are undoubtedly meteorological limitations since the water content is ultimately limited by the dynamics that can support it. These basic considerations suggest that N_t is potentially subject to greater variations over areas than is χ once an area becomes sufficiently large.

The structure of this work is first to present some observations of the RD of R, N_t, and χ over a set of measurements in rain over a small network of optical disdrometers. These observations are then explored using statistical fundamentals for sums such as (1). The observations then lead to the physical principles and mathematics behind why and what we are observing. These insights then allow us to consider what happens over domains much larger than the characteristic dimension of this network even in the absence of direct observations.

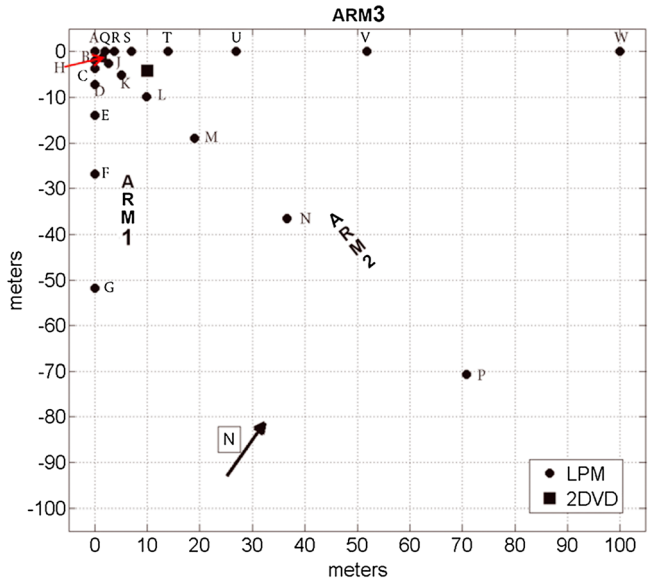

Figure 1. A schematic of the layout of the laser precipitation monitors (LPMs) (optical disdrometers) network with the letters referencing specific instruments as further discussed in the text. The 2-D video disdrometer (2DVD) is indicated by the square box. The origin of the network is taken to be at detector A in the upper left corner. The ARMS refer to specific linear arrays of instruments [*Jameson et al*., 2015a].

2. Preliminary Considerations

2.1. The Network of Detectors

As previously described in *Jameson et al*. [2015a] and repeated here for convenience, the network consists of 21 Thies Laser Precipitation Monitors (LPMs), in conjunction with a Joanneum compact two-dimensional video disdrometer (2DVD). The array is located at historic "Dixie Plantation" near Hollywood, SC; this property (owned by the College of Charleston Foundation) is used for a variety of ecological, educational, and research purposes. The site is located at 32°44′26″N and 80°10′36″W.

The instrument layout is shown in Figure 1 and was designed to develop a dense network with distinct spatial separations. This layout contrasts with the usual grid setup that collects a lot of information at only one particular separation distance but then abandons information on many other scales. By using logarithmic spacing, however, spatial scales from approximately 1 m to 100 m can be explored simultaneously. With the addition of the compact 2DVD (which is capable of resolving spatial locations of drops to within less than 1 mm), this array then allows us to investigate rainfall spatial variability through 5 orders of magnitude, most of which have not been extensively explored in past studies.

Each LPM was calibrated in a separate indoor laboratory and moved to the field site. This study uses data taken by 19 operational LPMs (LPMs *L* and *M* had a glitch in the wiring which was not rectified until early December 2013).

The Thies LPM instruments were characterized in detail by *Frasson et al*. [2011] and have been used in a number of other studies including *Brawn and Upton* [2008] and *Fernández-Raga et al*. [2009, 2010]. Optical disdrometers are well recognized as useful tools for characterizing drop size distributions [*Löffler-Mang and Joss*, 2000; *Tokay et al*., 2001]. It is not likely that the results presented here depend upon the type of disdrometer [*Islam et al*., 2012]. The LPMs are infrared occlusion instruments that can be run in several separate modes; for this study, the instruments were run in their default mode associated with 1 min integrations; in this mode, the device reports a spectrum each minute indicating how many droplets were detected in each of 22 disjoint drop size bins and 20 disjoint velocity bins (thus, each drop is characterized as belonging to 1 of 440 different categories). The known issues associated with particle sizing were mitigated to the greatest degree possible by verifying consistent performance in the lab before deployment and using identical instruments throughout the array. Moreover, measurements by all of the instruments were compared to minimize the inclusion of questionable behavior.

The devices are naturally synchronized; all devices were turned on simultaneously since they are powered with the same power supply. Although these devices are intended to be very low maintenance, the acquisition of data is reset every week to ensure minimal temporal drift; empirical estimation from this process suggests a relative shift of less than a second per week among all detectors. During the weekly maintenance activity, the devices are confirmed to be level, free of debris/insects, and recording properly.

The instruments are placed along three arms, two being orthogonal and the third bisecting the right angle. Eight instruments are spaced logarithmically out to 100 m along two of the arms, but the third arm having seven instruments only extends 52 m. This spacing provides increasing spatial resolution toward the network origin. Drop counts over 22 size bins are recorded every minute for all the instruments so that we can estimate the PSD of all the detectors every minute.

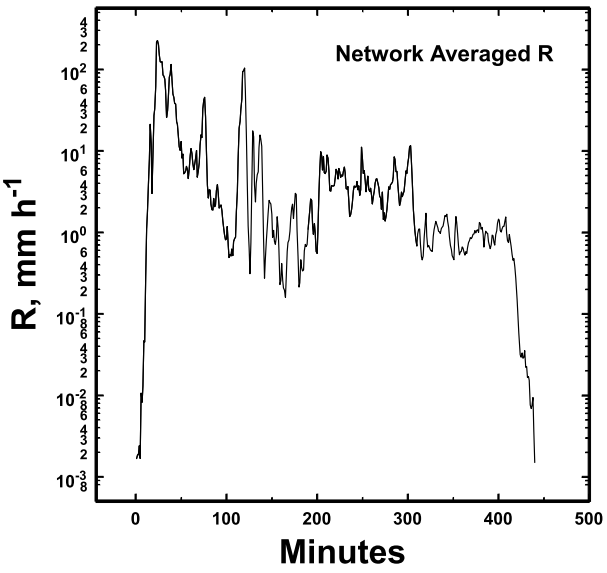

Figure 2. Network-averaged rainfall rate during the 440 min event.

From this entire grid extending out to 100 m, grids of other sizes can be constructed as well. In this study we consider a 2 m, 4 m, 7 m, 14 m, 27 m, 52 m, and the full grid containing all of the instruments out to 100 m. Other grids can, of course, be constructed, but because we wished to look at the changes associated with the expansion of a network size rather than its relocation, we have the larger grids containing the smaller subgrids.

2.2. The Meteorological Overview

The first rain event consisted of both a more intense convective component and a lighter more stratiform component that began on Saturday, 23 November 2013 16:45:00 UTC and lasted for 440 min with maximum rainfall rates approaching 250 mm h^{-1}. These data, therefore, cover a wide range of meteorological conditions so that the results presented below can be considered representative of many situations. In order to get a basic feeling for this rain event, the rainfall rate averaged over the entire network is illustrated in Figure 2. Only 19 of the 21 detectors were operational during this event (i.e., excluding detectors *L* and *M* as shown in Figure 1) so that this average is only over those disdrometers.

3. Data and Analyses

3.1. Relative Dispersions

We begin by looking at the average properties over the entire 440 min. First, each minute we calculate the standard deviations and mean values of both N_t and R using all the observations by all the disdrometers in the entire network. Figure 3 illustrates the linear correlation relation between σ_R and σ_{Nt}, while Figure 4 gives the relation between the mean rainfall rate $<R>$ and the average total number of drops $<N_t>$. Both relations are highly correlated, so we divide the relation in Figure 3 by that in Figure 4 to calculate that

$$\frac{\sigma_R}{<R>} = 1.3980\frac{\sigma_{N_t}}{<N_t>} \quad \text{or} \quad \frac{\mathrm{RD}_R}{\mathrm{RD}_{N_t}} = 1.3980 \tag{2}$$

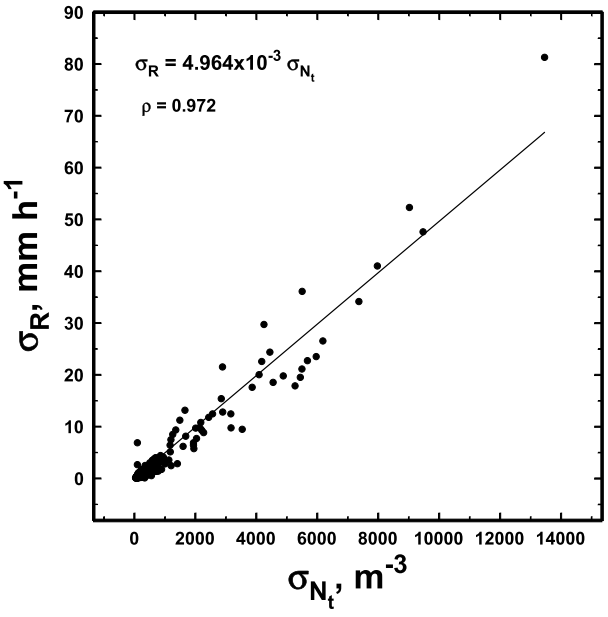

Figure 3. The 1 min 100 m network standard deviation of the rainfall rate, σ_R, versus the 1 min 100 m network standard deviation of the total number of drops, N_t, over the entire interval.

To see how well this simple relation represents the average conditions, the minute by minute observed $\mathrm{RD}_R/\mathrm{RD}_{Nt}$ are plotted (black line) in Figure 5 along with the average value (magenta line). Remarkably, the oscillations of individual minute values are all around the average value of 1.3994 which is within 0.01% of the value in (2) and, most

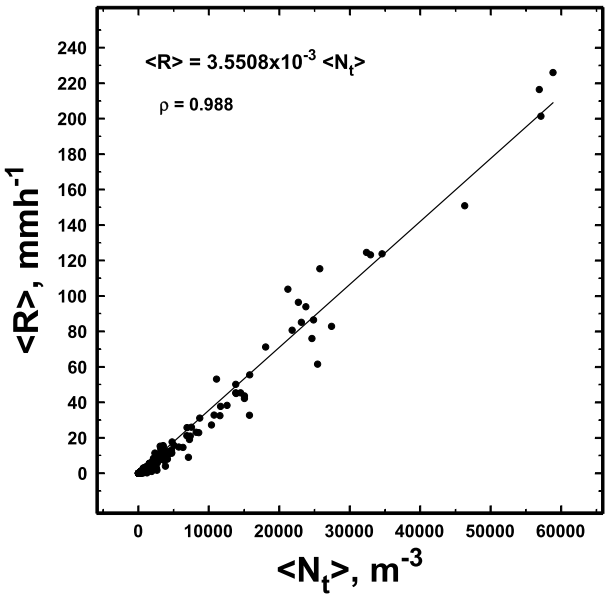

Figure 4. The 1 min network average rainfall rate $<R>$ versus the 1 min network average of the total number of drops $<N_t>$ over the entire interval.

importantly, it is nearly constant regardless of the different meteorological conditions as represented by the network average rainfall rate (red line).

To explore how this might be happening, we briefly review some earlier work. *Jameson and Kostinski* [2001] developed the following relationship between RD_R and RD_{Nt}, namely,

$$RD_R = \left[\frac{< N_t > F\sigma_\chi^2}{\sigma_{N_t}^2}\frac{}{\langle\chi\rangle^2} + 1\right]^{\frac{1}{2}} RD_{N_t} \quad (3)$$

where $F = <(\sigma^2[R|N_t])>/\{<N_t>\sigma^2[\chi]\}$ and $<(\sigma^2[R|N_t])>$ is the variance of R for constant N_t. As explained in *Jameson and Kostinski* [2001] F accounts for any correlation that might be present between N_t and χ. For 1 min values, $F \sim 1$; i.e., the two quantities are essentially statistically independent as Figure 5 illustrates. However, over an entire period of observations F can become much larger; i.e., N_t and χ can become more correlated as we shall see. An important point to note is that any effect from the drop size distribution is contained within the coefficient under the square root.

Equation (3) can be used to calculate the relation between RD_R and RD_{Nt}. In particular, the minute by minute relation between RD_R and RD_{Nt} using the network values of N_t and χ, realizing that measurement statistical fluctuations can introduce uncertainties [e.g., *Uijlenhoet et al*., 2006], is illustrated in Figure 5 by the green line. While the agreement with observations is not perfect given the measurement uncertainties, we feel that it is sufficient ($\rho = 0.84$) to justify its continued use in this work.

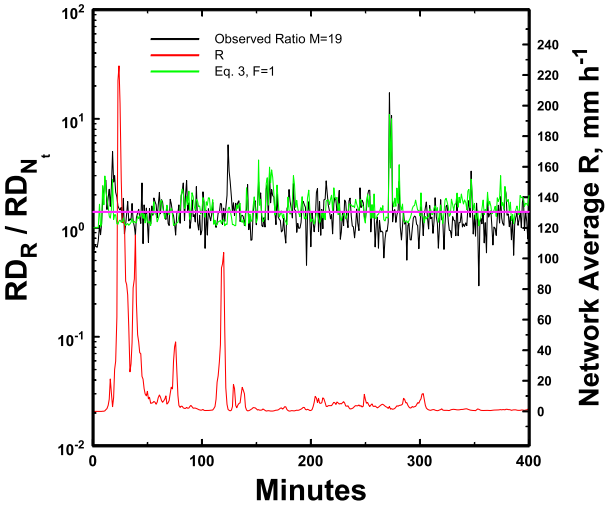

Figure 5. The observed minute by minute (black line) ratio, R, of the relative dispersion of the rainfall rate to that for the total number of drops as a function of time over the entire network. The green line is that computed using (3) and the observed 1 min network values of $<N_t>$, σ^2_{Nt}, and relative dispersion of χ. The magenta line is the mean ratio of R. The red line is the network average rainfall rate illustrating that the steadiness of R is not particularly sensitive to changes in the meteorology.

The average ratio of RD_R/RD_{Nt}, however, depends upon the dimension of the network. (Note that this curve is not well fit by a power law and that the limited dynamic ranges of both axes in this figure as well as in Figures 7 and 12 are insufficient for statistically reliable power law fits [*Stumpf and Porter*, 2012].) While it is tempting to attribute this to the number of instruments in each grid (M), the ratio minimizes such a potential effect as illustrated in Figure 6. For the smallest network, there are four detectors, while for the largest network, there are 19 detectors so that for a purely M effect one would expect that the smallest grid value would drop to 1.01 at the 100 m network dimension. Obviously, this does not happen so we know that something else is going on, nor is it a partial network filling effect [*Jameson et al*., 2015b], since all detectors contained drops throughout the 400 min interval.

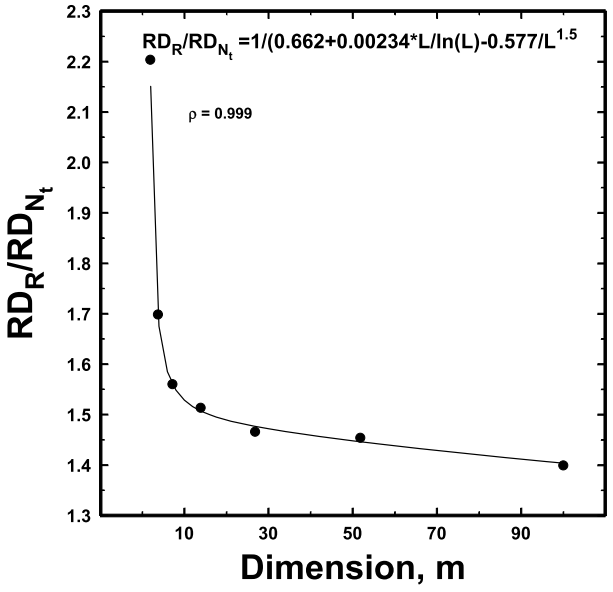

Figure 6. Ratio of the relative dispersion of the rainfall rate RD_R to the relative dispersion of the total number of drops RD_{Nt} as a function of the dimension of the network, L.

To understand what is happening, the variables σ^2_{Nt}, $<N_t>$, RD_χ, and F in the coefficient of (3) were computed for all the different sizes of networks as plotted in Figure 7. Whereas three of the variables remain nearly constant, the one that steadily increases is σ^2_{Nt}. Consequently, the coefficient in (3) steadily decreases as the dimension of the network increases. There is a physical reason for this.

3.2. A Physical Interpretation

To understand why the variance of N_t increases with network dimension, let us first consider what happens for just one drop size. As discussed in *Kostinski and Jameson* [1999] and as repeated here from *Jameson et al.* [2015b], the drop concentration at one size can be expressed as $n = N_t \times P(D)$, where $P(D)$ is the probability distribution of the drops versus drop diameter. As originally discussed in *Jameson et al.* [2015b] for drops of a single size, given a reasonable number of detectors to adequately sample over an area, the contributions to the variance (σ^2_n) of n are increased by all spatial wavelengths being sampled by the network. If we just consider a simple sinusoidal wave having amplitude a_i modulating around the mean concentration, the variance will be proportional to $|a_i|^2$. As the dimension of the area increases, the net variance will be proportional to the sum of all the amplitudes weighted by their spectral contributions. Hence, as the dimension of the area increases, σ^2_n will increase monotonically as the size of the area increases at least up until approximately a wavelength of about one half the characteristic dimension of the area, if such wavelengths are present. While this cutoff is not rigid, longer wavelengths contribute mostly to the mean value which is subtracted when computing the variance. Another way to think of it is that the network acts to integrate the variance spectrum of the spatial correlation function of n (the correlation between n at two different spatial locations) from the highest (smallest) toward lower (longest) frequencies (wavelengths) as the characteristic dimension of the network increases.

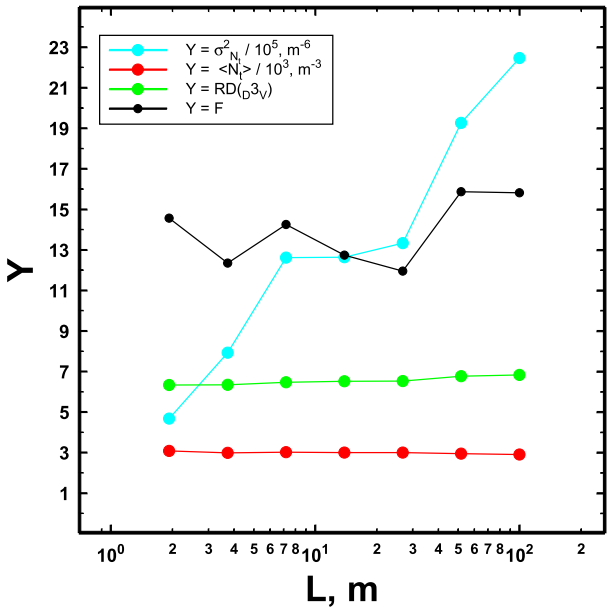

Figure 7. Plots of network averages of variables discussed in the text over the entire period of observations as functions of the network dimension L. Only the variance of N_t shows marked dependence on L.

The new twist with regard to the rainfall rate is that it simultaneously involves drops of different sizes. When multiple drop sizes are present, the same argument as above applies to the ith drop size for all n_i. Specifically, if the numbers of drops at all the different sizes were all mutually statistically independent from

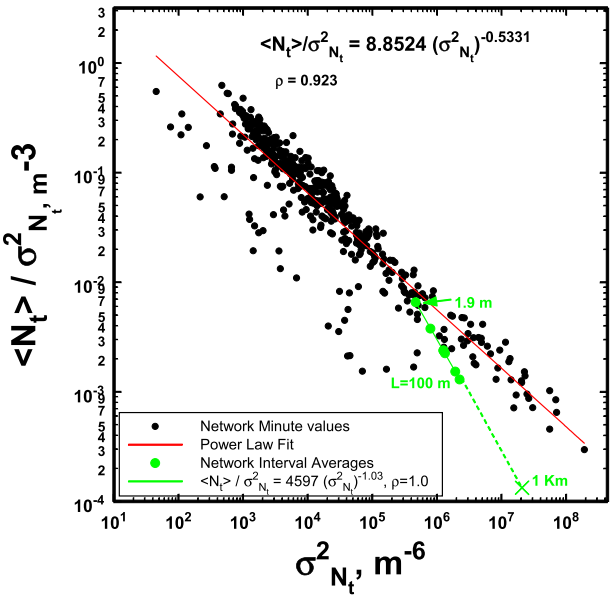

Figure 8. The ratio of the average total number of particles $<N_t>$ to the variance of N_t for both the 1 min values over the 100 m network (black) and for the network average values over the entire interval for different network dimensions (green) as discussed further in the text.

minute to minute, then because $N_t = \Sigma\, n$, it follows from the Bienaymé formula [*Loève*, 1977] that $\sigma^2_{N_t} = \sum_i \sigma^2_{n_i}$, where $\sigma^2{}_{ni}$ are the variances associated with each D_i. If the n_i are positively correlated, as is often the case at least on temporal scales of 1 min or less [*Jameson and Kostinski*, 1999, 2000], then the variance is enhanced to even larger values by the term $2\sum_{1\le i}\sum_{<j\le n} \mathrm{Cov}(n_i, n_j)$, where Cov is the covariance function. Therefore, we conclude that $\sigma^2{}_{Nt}$ should increase monotonically as the network size increases. Hence, the finding illustrated in Figure 7 is likely quite general and not peculiar to this particular set of measurements as illustrated again later.

3.3. Further Consideration of (3)

Returning to (3), it appears that as the network size increases, the coefficient will be dominated by the ratio $\Re = < N_t > /\sigma^2_{N_t}$. For the 1 min observations, this ratio decreases approximately as $1/\sigma_{Nt}$ as illustrated in Figure 8 so that as the dimension of an area increases, $\sigma^2{}_{Nt}$ increases and $\Re$ decreases. For the network averages over the entire observation period, $\Re$ decreases even more rapidly, namely, as $1/\sigma^2{}_{Nt}$, perhaps reflecting increased contributions of all the appropriate wavelengths to $\sigma^2{}_{Nt}$ during the entire 400 min interval. On the other hand, RD_χ can only become only so large because the terminal fall speed and the drop sizes are finite so that as Figure 7 suggests, it will not be a function of the size of the domain, although its value will likely be different from that in Figure 7 depending upon the meteorological circumstances. Finally, the factor F that reflects the degree of correlation between the variables N_t and χ increases from approximately unity for the 1 min observations to around 14 apparently because of increased correlation over the entire time period. While its value is also likely to change depending on the meteorological circumstances, Figure 7 suggests that like RD_χ, it is not a strong function of the dimension of the area. Consequently, quite generally, at some sufficiently large dimension, the coefficient in (3) will become dominated by $\Re$.

Unfortunately, we do not have measurements out to a sufficient distance to observe this directly. However, it is still possible to explore what happens using a few scientifically based assumptions. While this extrapolation itself remains to be validated, we feel it is worth pursuing in order to explore, at least, how the areal dimensions are likely to affect the rainfall rate variability. While some may feel that such an extrapolation is unjustified, we remind the reader that this is no more exceptional than in past and current studies when small-scale measurements of raindrop size distributions were and are extrapolated to much larger scales without any attempt at validation. At least here we are trying to do so. While validation must await the availability of disdrometer measurements of individual rain events over larger scales coincident with small-scale observations such as these, we proceed by using the only known spatial correlation function for disdrometers out to 1 km for the rainfall rate found by *Jaffrain and Berne* [2012] applicable to their wide range of convective and stratiform rain events. Correlation functions extending several kilometers based upon tipping bucket rain gages over 30 min integration times show similar stretched exponential functional forms [*Tokay et al.*, 2013]. The observed spatial correlation functions of drop concentrations out to 100 m reported recently in *Jameson et al.* [2015a] are also consistent with this spatial correlation function. Using R as a proxy for N_t, as Figure 4 suggests is reasonable, we take the stretched exponential function proposed by *Jaffrain and Berne* [2012], namely,

$$\rho(L) = C \exp\left[-\left(\frac{L}{1.949}\right)^p\right] \tag{4}$$

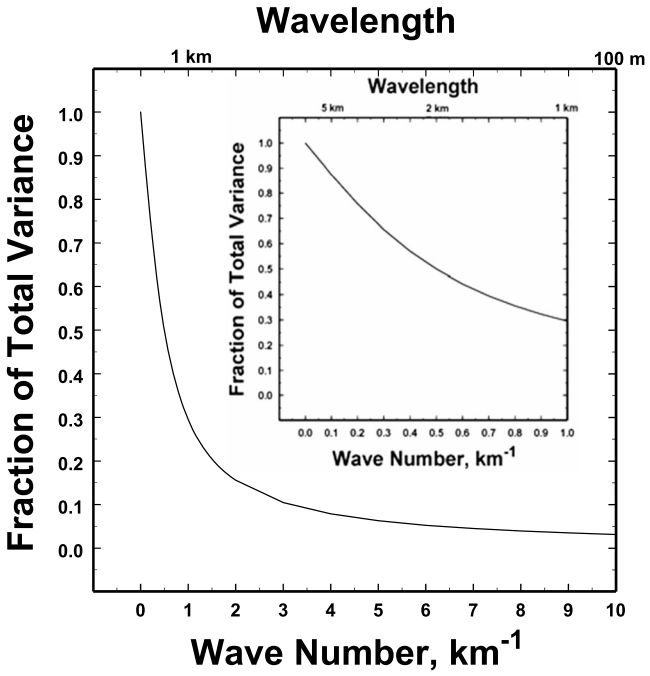

Figure 9. The cumulative distribution function of the Lorentzian variance spectrum of N_t derived from the Fourier transform of an exponentially decreasing spatial correlation distance having a 1/*e* distance of 2 km as discussed in the text. Most of the variance lies at dimensions greater than a few hundred meters. This is discussed further in the text.

where L is in kilometers, C is a constant, and $p = 1.32$. When $p = 1$, this becomes an exponential function, and when $p = 2$, this becomes a Gaussian so that (4) lies in between. According to standard Fourier transform theory [e.g., *Blackman and Tukey*, 1975] the Fourier transform of the spatial correlation function yields the variance spectrum. However, since there is no closed form solution for the Fourier transform of (4), we simplify (4) to be an exponential of the form

$$\rho(L) = \exp\left[-\frac{L}{2}\right] \tag{5}$$

The Fourier transform of (5) then yields a Lorentzian variance spectrum having a cumulative distribution function (CDF) given by

$$\mathrm{CDF} = 1 - \frac{2\arctan(2\kappa)}{\pi} \tag{6}$$

where κ is the wave number km^{-1} as plotted in Figure 9. This is an analytic expression requiring no power law fits. For this example, at 100 m we would only see about 3% of all of the variance. At 1 km, however, we would see almost 30% of all the variance so that at 1 km σ^2_{Nt} would be about 10 times larger than what is observed at 100 m. Using that number, the expression in the legend of Figure 9, and (3) the mean values of RD_χ and F in Figure 7, we have that $\mathrm{RD}_R/\mathrm{RD}_{Nt} \cong 1.04$. In other words, by a dimension of 1 km, the variability in the drop size distribution vis-à-vis χ contributes only about 4% to the total variability of R with the remainder coming from the variability in N_t. For a 2 km dimension $\mathrm{RD}_R/\mathrm{RD}_{Nt} \cong 1.02$ so that by the time the dimension approaches kilometer sizes, $\frac{\sigma_R}{<R>} \approx \frac{\sigma_{N_t}}{<N_t>}$ as illustrated in Figure 10 for these conditions.

This has the potential of simplifying the modeling of the rainfall rate over areas larger than around a kilometer, for example, because all one needs are drop counts and an average value for the rainfall rate with no need for detailed spatial observations of the DSD. That is,

$$E(R) = E(N_t)E\left(D^3V_t\right) \tag{7}$$

where the E variables denote the expected values estimated from the averages so that

$$E\left(D^3V_t\right) = \frac{E(R)}{E(N_t)} \tag{8}$$

This is the coefficient needed to translate N_t into R as illustrated in Figure 4. Consequently, by observing the average $<N_t>$ and $<R>$ over an area over an interval one can convert the observed values of N_t into R without direct reference to any DSD. Similarly, with respect to modeling, one can specify $<N_t>$ and $<R>$ and then specify the statistical properties of N_t (i.e., the spatial correlation function and distribution function as discussed in *Jameson* [2015]). One can then generate 2-D fields of R which are physically meaningful again, without having to refer to specific DSD and while preserving the relative dispersion of R consistent with (3).

It also suggests that the method of using deviations of radar signal statistics of the radar reflectivity factor, $Z = \Sigma D^6$, from Rayleigh statistics [*Jameson*, 2008] for determining the variability of the rainfall rates is also likely useful. Calculations using the data here indicate that $\mathrm{RD}_Z/\mathrm{RD}_R \cong 1.10$ at 1 km and 1.06 at 2 km so that the results in *Jameson* [2008] are likely meaningful. However, to be sure, all of these calculations are only

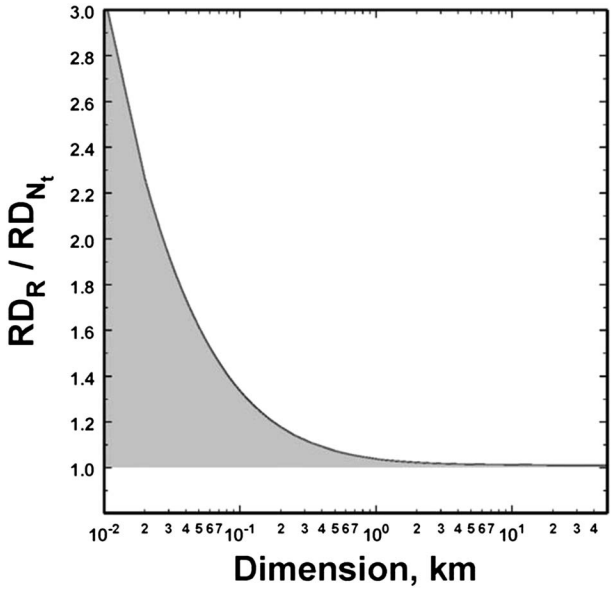

Figure 10. The ratio of the relative dispersion of the rainfall rate, RD_R, to that for the total number of drops, RD_{Nt}, as a function of dimension for the conditions described in the text. The shaded region denotes where the drop size distribution influences the ratio through the relative dispersion of χ. Note that for dimensions greater than around 1 km, the drop size distribution has little effect on this ratio.

suggestive, and there remains a need for more observations of the spatial correlation functions on scales of 1 km and greater.

3.4. A Second Case

In the case above, there is a strong convective component. In this section we consider a more uniform rain with significantly smaller variance of N_t and over a significantly shorter duration of only 80 min compared to the much longer previous example. These data were collected on 26 December 2013 beginning at 17:47 UTC. As the rain rate profile indicates (Figure 11), there was a background of light rain (around 1–2 mm h^{-1}) with a few short bursts of heavier rain of up to 7 mm h^{-1}. Thus, this much shorter rain event is much less intense and much less variable than the previous case.

Following the procedures described above, as in Figure 7, once again the only variable that is a significant function of the network dimension L is σ^2_{Nt} as illustrated in Figure 12. Moreover, as in Figure 8, we see in Figure 13 quite similar functions for $\Re = < N_t > /\sigma^2_{N_t}$ both for minute values and for network interval averages. Because of the broad range of meteorological conditions observed by *Jaffrain and Berne* [2012], the spatial correlation function and its Fourier transform variance spectrum are again used to understand these observations. Following the procedures in the previous case, we conclude for these data that $RD_R/RD_{Nt} \cong 1.06$ and 1.04 for $L = 1$ and 2 km, respectively. These values, then, are quite similar to those above of 1.04 and 1.02 even though the conditions and length of observation are considerably different. This, then, provides some confidence in concluding that over larger domains, the variability of the rainfall rate is largely determined by the variability in the number of drops with DSD variability playing a much, much less significant role. Thus, for many purposes it is not necessary to include drop size variability when estimating or when modeling rainfall rate variability over kilometer and larger domains. On the other hand, the variability of the DSD plays an increasingly important role over domains of just several meters. That may explain, in part, why DSD variability achieved such prominence in the analyses of point measurements of

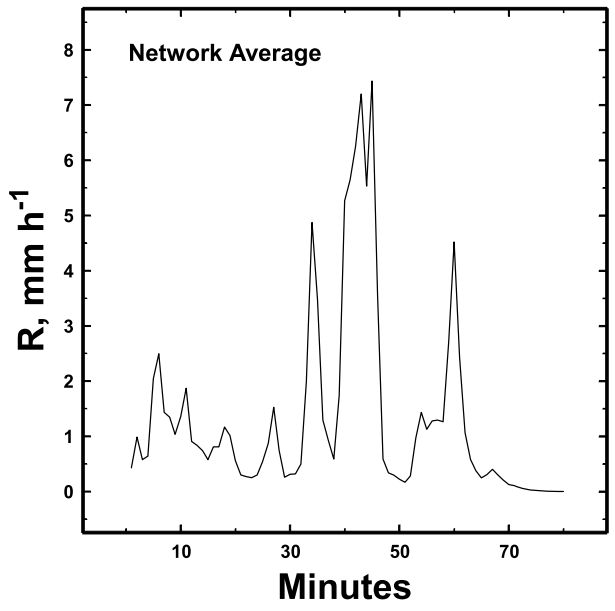

Figure 11. The network average rainfall rate for a second case of rain as discussed in the text [from *Jameson et al.*, 2015a].

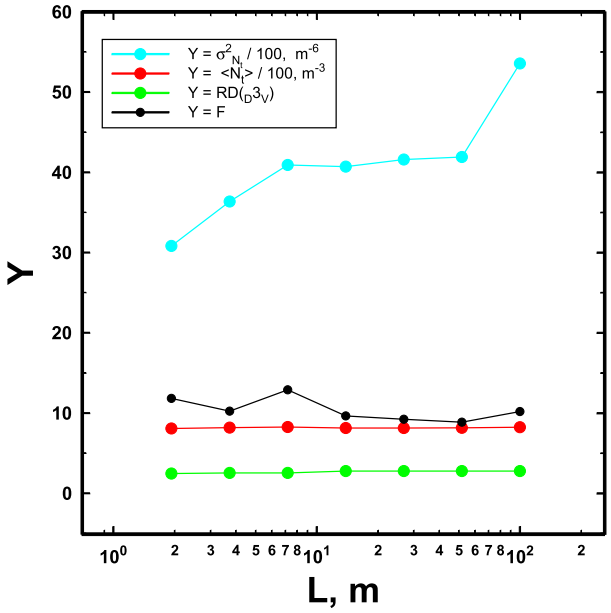

Figure 12. Plots of the average intrinsic PSD and that observed over the entire network. The red filled area illustrates the spread associated with the intrinsic PSD. Note that the mean curve for the entire network falls outside this region for drops larger than 4 mm diameter.

the rainfall rate in historic work. This importance, however, now appears to have been an unvalidated extrapolation to the larger domains such as those observed by remote sensing instruments and those output from many numerical models.

4. Summary

A drop size distribution can be expressed as DSD = $N_t \times P(D) = N_t \times PSD$. The variability of the rainfall rate, then, derives from two sources, namely, the variability of PSD and the variability of N_t. Most past studies using a few instruments in close proximity suggested that the PSD was most important to the observed variability of R although *Uijlenhoet et al.* [2003] found that indeed, N_t dominated the variability during extreme rainfall even over small regions. What this work shows, however, is that while the PSD and N_t may often play about equal roles over small sampling domains up to tens of meters, the role of N_t overwhelms the PSD contribution as the size of the domain increases to kilometer scales.

The reason for this is that drop sizes (D) and their terminal fall speeds (V_t) are severely limited regardless of domain size; N_t is not. Consequently, as the size of a domain increases, it acts to integrate over an ever increasing number of wavelengths of the variance spectrum of N_t derived from the Fourier transform of the spatial correlation function. Hence, while the variability of the PSD and the terminal fall speeds are then only weak functions of the size of a domain, σ^2_{Nt} continuously increases with size.

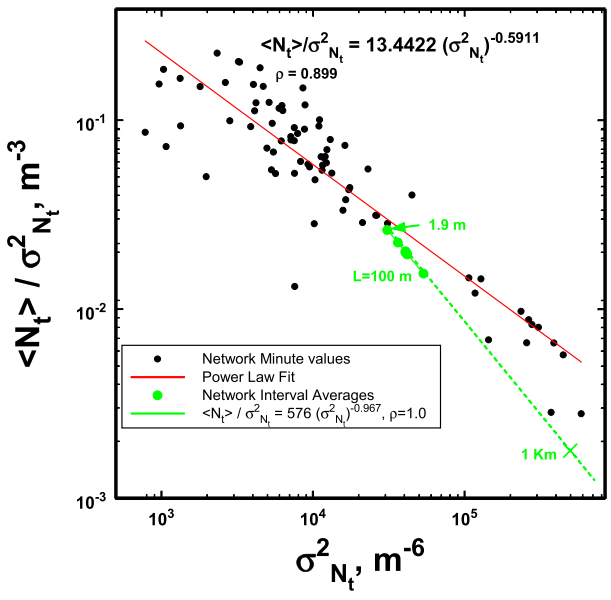

Figure 13. Similar to Figure 8 except for the second 80 min rain case as discussed in the text.

The relationships between the variability of the rainfall rate and those of the PSD and N_t are conveniently expressed using their relative dispersions as given in (3) which reveals that the role of the relative dispersion of χ is weighted by the ratio of $\langle N_t \rangle / \sigma^2_{Nt}$, where $\langle\rangle$ denotes the average over a domain of dimension L. Measurements over different sizes of networks for two different sets of data reveal that this ratio is a nearly linearly decreasing function of σ^2_{Nt} so that the relevance of the relative dispersion of χ also decreases rapidly with increasing L. While these observations were limited to 100 m scales, with reasonable justification we can use the variance spectrum associated with an exponentially decreasing spatial correlation to argue that once a domain size reaches kilometer scales, the relative dispersions of the rainfall rates are

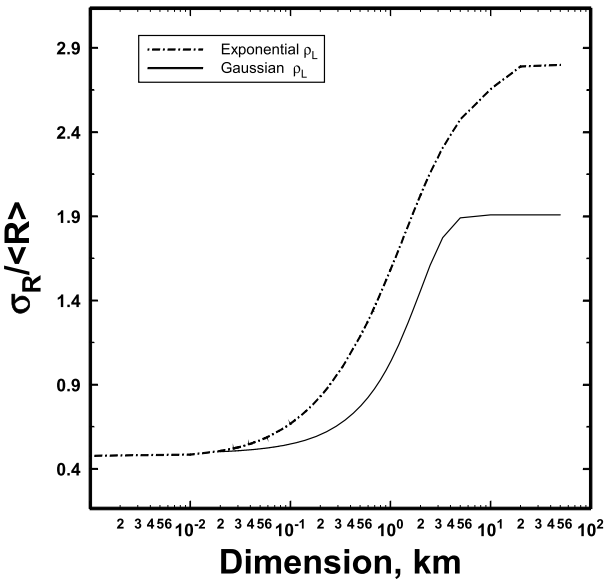

Figure 14. The spectrum of the relative dispersion of the rainfall rate using the 100 m network observations from the first data set and assuming an exponentially decreasing spatial correlation function of the total number of drops, N_t, as discussed in the text. Multiplication by the mean rainfall rate $<R>$ gives the spectrum of σ_R. The corresponding curve for a Gaussian spatial correlation function is also included. The stretched exponential (4) will lie between these two curves.

nearly equal of those of N_t alone to within 2–6% for 1 km scale with decreasing differences out to ever larger domains.

As discussed earlier, this means that a physically based numerical modeling of rainfall rate over sufficiently large domains (i.e., at sufficiently coarse resolution) need only be concerned with N_t and the selection of a value of $<N_t>/<R>$ which acts as a proxy for $<\chi>$. Conversely, these disdrometer network observations and an understanding of the role of the spatial correlation function can be used to produce a spectrum of the relative dispersion of the rainfall rate $\sigma_R/<R>$ using (3) over a large range of dimensions as illustrated in Figure 14. Multiplication by $<R>$ readily converts Figure 14 into the spectrum of σ_R. Thus, as the dimension of an area increases, that area effectively integrates over ever increasing wavelengths of the variance spectrum of N_t that in turn gives rise to this increase in σ_R as an area expands. Figure 14 suggests an upper limit of σ_R to be 2 to 3 times the mean rainfall rate for $L = 2$ km at least in this analysis..

Moreover, radar measurements of the variability of the intrinsic radar reflectivity factor (Z_i) obtained after accounting for Rayleigh signal fluctuations [*Jameson*, 2008] can be used to estimate the relative dispersion of the rainfall rates to within around 10% at 1 km resolution without the need for any *Z-R* relation as illustrated in Figures 6 and 7 in *Jameson* [2008]. Thus, the need to focus on drop size distributions and their variability depends upon the research objectives, but for resolutions larger than around a kilometer, at least, a detailed understanding of the drop size distributions simply is not required for understanding the variability in the rainfall rates.

As noted by some readers, most *Z-R* relations are not linear as the linearity discussed above would seem to imply. First, it is first important to remember that many of the nonlinear *Z-R* relations of dubious merit given that they are derived using single disdrometer measurements with inadequate sampling of drop counts. However, to be fair, strict linearity among the variables such as Z and R and N_t applies to statistically homogeneous data. As these data show (Figure 4; for a 23 h data set, also see *Jameson* [2015, Figure 12]), however, statistical heterogeneity can still be described by a linear relation because there is still an average χ such that $R \propto N_t$ as discussed in *Jameson et al.* [2015a, pp. 1660–1661]. However, the scatter around such a linear relation will likely increase as an area increases because the statistical heterogeneity likely increases. Consequently, over large areas it may well be that nonlinear fits can reduce the total scatter when there is disparately statistically heterogeneous data. However, they do not represent a challenge to the conclusions reached here. It must be remembered that statistical fits are *not* based upon fundamental physics in spite of the prevalence of such misconceptions in the literature. Rather, such fits mean that when one statistically combines widely different data, there may well be better, more useful empirical statistical fits with lower scatter than a linear one, but, unlike linear relations, such fits are not physically based.

To get a better feel for this, it often appears that statistical heterogeneity can be represented by a combination of statistically homogeneous components [*Jameson*, 2007]. In that case a plot of N_t versus R would reveal distinct clusterings of points, each with its own linear relation. Yet there would still be an "average" linear relation splitting these lines depending upon how each is contributing to the mean χ. This average relation

is still valid, but a nonphysically based nonlinear fit might well provide a better statistical fit. However, just because one goes so far enough out that a DSD changes significantly at some remote location does not mean that the DSD has become a more important contributor to the variability of the rainfall rate than N_t.

One can always apply this approach to other kinds of observations such as those by radar and vertical profilers. In the paper we use some radar measurements of such applications. While dual-polarization measurements have their place, they do not provide direct measurements of the DSD nor of N_t which must be inferred under different assumptions. Consequently, any results from such analyses would have to be viewed cautiously. Profiler observations provide more direct observations, although they too are subject to some assumptions. If they have sufficient temporal resolution, they could be used to conduct similar interesting studies in the vertical plane.

Regardless of such considerations, it is clear that the variability in the rainfall rate, while depending upon both the variability in the PSD and N_t in small domains, increases as the size of the domain increases until it is totally dominated by the variability of N_t. The scale at which this occurs depends upon the particular correlation function. For that function reported in *Jaffrain and Berne* [2012] using an entirely different set of data than analyzed here, that distance is 1 km so that beyond that distance, the variability in the PSD is not important. The mean PSD, however, remains important through its various average moments.

Acknowledgments
This work was supported by the National Science Foundation (NSF) under grants AGS130087 and AGS1532423 as well as by the United States Social Security Administration. Support for M.L. came from the National Science Foundation under grants AGS-1230240 and AGS1532977. The authors are also especially grateful to the students of Larsen, namely, Joerael Harris, Robert Lemasters, Katelyn O'Dell, Joshua Teves, and Michael Chute who diligently worked to make this network a functioning reality. The data funded by the NSF are public domain and may be obtained by contacting the authors.

References

Best, A. C. (1950), The size distribution of raindrops, *Q. J. R. Meteorol. Soc.*, *76*(327), 16–36, doi:10.1002/qj.49707632704.
Blackman, R. B., and J. W. Tukey (1975), *The Measurement of Power Spectra From the Point of View of Communications Engineering*, Dover Publ, New York.
Brawn, D., and G. Upton (2008), On the measurement of atmospheric gamma drop-size distributions, *Atmos. Sci. Lett.*, *9*(4), 245–247, doi:10.1002/asl.198.
Caracciolo, C., M. Napoli, F. Porcù, F. Prodi, S. Dietrich, C. Zanchi, and S. Orlandini (2012), Raindrop size distribution and soil erosion, *J. Irrig. Drain. Eng.*, *138*(5), 461–469, doi:10.1061/(ASCE)IR.1943-4774.0000412.
Frasson, R. P., L. K. da Cunha, and W. F. Krajewski (2011), Assessment of the Thies optical disdrometer performance, *Atmos. Res.*, *101*(1–2), 237–255, doi:10.1016/j.atmosres.2011.02.014.
Fernández-Raga, M., A. Castro, C. Palencia, A. I. Calvo, and R. Fraile (2009), Rain events on 22 October 2006 in León (Spain): Drop size spectra, *Atmos. Res.*, *93*(1–3), 619–635, doi:10.1016/j.atmosres.2008.09.035.
Fernández-Raga, M., R. Fraile, J. J. Keizer, M. E. Varela Teijeiro, A. Castro, C. Palencia, A. I. Calvo, J. Koenders, and R. L. Da Costa Marques (2010), The kinetic energy of rain measured with an optical disdrometer: An application to splash erosion, *Atmos. Res.*, 225–240, doi:10.1016/j.atmosres.2009.07.013.
Islam, T., M. A. Rico-Ramirez, M. Thurai, and D. Han (2012), Characteristics of raindrop spectra as normalized gamma distribution from a Joss–Waldvogel disdrometer, *Atmos. Res.*, *108*, 57–73, doi:10.1016/j.atmosres.2012.01.013.
Jaffrain, J., and A. Berne (2012), Quantification of the small-scale spatial structure of the raindrop size distribution from a network of disdrometers, *J. Appl. Meteorol. Climatol.*, *51*(5), 941–953, doi:10.1175/JAMC-D-11-0136.1.
Jameson, A. R. (2007), A new characterization of rain and clouds: Results from a statistical inversion of count data, *J. Atmos. Sci.*, *64*(6), 2012–2028, doi:10.1175/JAS3950.1.
Jameson, A. R. (2008), Radar observations of rainfall variability using non-Rayleigh signal fluctuations, *J. Appl. Meteorol. Climatol.*, *47*(2), 607–619, doi:10.1175/2007JAMC1630.1.
Jameson, A. R. (2015), A Bayesian method for upsizing single disdrometer drop size counts for rain physics studies and areal applications, *IEEE Trans. Geosci. Remote Sens.*, *53*(1), 335–343, doi:10.1109/TGRS.2014.2322092.
Jameson, A. R., and A. B. Kostinski (1999), Fluctuation properties of precipitation. Part V: Distribution of rain rates—Theory and observations in clustered rain, *J. Atmos. Sci.*, *56*(22), 3920–3932, doi:10.1175/1520-0469(1999)056<3920:FPOPPV>2.0.CO;2.
Jameson, A. R., and A. B. Kostinski (2000), Fluctuation properties of precipitation. Part VI: Observations of hyperfine clustering and drop size distribution structures in three-dimensional rain, *J. Atmos. Sci.*, *57*(3), 373–388, doi:10.1175/1520-0469(2000)057<0373:FPOPPV>2.0.CO;2.
Jameson, A. R., and A. B. Kostinski (2001), Reconsideration of the physical and empirical origins of Z–R relations in radar meteorology, *Q. J. R. Meteorol. Soc.*, *127*(572), 517–538, doi:10.1002/qj.49712757214.
Jameson, A. R., and A. B. Kostinski (2002), Spurious power-law relations among rainfall and radar parameters, *Q. J. R. Meteorol. Soc.*, *128*(584), 2045–2058, doi:10.1256/003590002320603520.
Jameson, A. R., M. L. Larsen, and A. B. Kostinski (2015a), Disdrometer network observations of finescale spatial–temporal clustering in rain, *J. Atmos. Sci.*, *72*(4), 1648–1666, doi:10.1175/JAS-D-14-0136.1.
Jameson, A. R., M. L. Larsen, and A. B. Kostinski (2015b), On the variability of drop size distributions over areas, *J. Atmos. Sci.*, *72*(4), 1386–1397, doi:10.1175/JAS-D-14-0258.1.
Kinnell, P. I. A. (2005), Raindrop-impact-induced erosion processes and prediction: A review, *Hydrol. Processes*, *19*(14), 2815–2844, doi:10.1002/hyp.5788.
Kostinski, A. B., and A. R. Jameson (1999), Fluctuation properties of precipitation. Part III: On the ubiquity and emergence of the exponential drop size specstra, *J. Atmos. Sci.*, *56*(1), 111–121, doi:10.1175/1520-0469(1999)056<0111:FPOPPI>2.0.CO;2.
Laws, J. O., and D. A. Parsons (1943), The relation of raindrop-size to intensity, *Eos Trans. AGU*, *24*(2), 452–460, doi:10.1029/TR024i002p00452.
Loève, M. (1977), *Probability Theory*, *Grad. Texts Math.*, vol. 45-46, 4th ed., Springer, New York.
Löffler-Mang, M., and J. Joss (2000), An optical disdrometer for measuring size and velocity of hydrometeors, *J. Atmos. Oceanic Technol.*, *17*(2), 130–139, doi:10.1175/1520-0426(2000)017<0130:AODFMS>2.0.CO;2.
Lovejoy, S., and B. B. Mandelbrot (1985), Fractal properties of rain, and a fractal model, *Tellus A*, *37A*(3), 209–232, doi:10.1111/j.1600-0870.1985.tb00423.x.

Marshall, J. S., and W. M. K. Palmer (1948), The distribution of raindrops with size, *J. Meteorol.*, *5*(4), 165–166, doi:10.1175/1520-0469(1948)005<0165:TDORWS>2.0.CO;2.

Meusburger, K., A. Steel, P. Panagos, L. Montanarella, and C. Alewell (2012), Spatial and temporal variability of rainfall erosivity factor for Switzerland, *Hydrol. Earth Syst. Sci.*, *16*(1), 167–177, doi:10.5194/hess-16-167-2012.

Sangati, M., and M. Borga (2009), Influence of rainfall spatial resolution on flash flood modelling, *Nat. Hazards Earth Syst. Sci.*, *9*(2), 575–584, doi:10.5194/nhess-9-575-2009.

Smith, M. B., V. I. Koren, Z. Zhang, S. M. Reed, J.-J. Pan, and F. Moreda (2004), Runoff response to spatial variability in precipitation: An analysis of observed data, *J. Hydrol.*, *298*(1–4), 267–286, doi:10.1016/j.jhydrol.2004.03.039.

Steiner, M., J. A. Smith, and R. Uijlenhoet (2004), A microphysical interpretation of radar reflectivity–rain rate relationships, *J. Atmos. Sci.*, *61*(10), 1114–1131, doi:10.1175/1520-0469(2004)061<1114:AMIORR>2.0.CO;2.

Stumpf, M. P. H., and M. A. Porter (2012), Critical truths about power laws, *Science*, *335*(6069), 665–666, doi:10.1126/science.1216142.

Tokay, A., A. Kruger, and W. F. Krajewski (2001), Comparison of drop size distribution measurements by impact and optical disdrometers, *J. Appl. Meteorol.*, *40*(11), 2083–2097, doi:10.1175/1520-0450(2001)040<2083:CODSDM>2.0.CO;2.

Tokay, A., R. J. Roche, and P. G. Bashor (2013), An experimental study of spatial variability of rainfall, *J. Hydrometeorol.*, *15*(2), 801–812, doi:10.1175/JHM-D-13-031.1.

Uijlenhoet, R., J. A. Smith, and M. Steiner (2003), The microphysical structure of extreme precipitation as inferred from ground-based raindrop spectra, *J. Atmos. Sci.*, *60*(10), 1220–1238, doi:10.1175/1520-0469(2003)60<1220:TMSOEP>2.0.CO;2.

Uijlenhoet, R., J. M. Porrà, D. S. Torres, and J.-D. Creutin (2006), Analytical solutions to sampling effects in drop size distribution measurements during stationary rainfall: Estimation of bulk rainfall variables, *J. Hydrol.*, *328*(1–2), 65–82, doi:10.1016/j.jhydrol.2005.11.043.

Uri, N. D., and J. A. Lewis (1999), Agriculture and the dynamics of soil erosion in the United States, *J. Sustainable Agric.*, *14*(2–3), 63–82, doi:10.1300/J064v14n02_07.